frontiers in Chemistry

ORIGINAL RESEARCH
published: 14 November 2019
doi: 10.3389/fchem.2019.00776

Bracelet-Like $Ni_{0.4}Cu_{0.6}O$ Microstructure Composed of Well-Aligned Nanoplatelets as a Superior Catalyst to the Hydrolysis of Ammonia Borane

Xianfeng Li[1]*, *Liucheng Gui*[2]* and *Huahong Zou*[2]

[1] School of Chemistry and Materials Engineering, Huizhou University, Huizhou, China, [2] State Key Laboratory for Chemistry and Molecular Engineering of Medicinal Resources, School of Chemistry and Pharmacy, Guangxi Normal University, Guilin, China

OPEN ACCESS

Edited by:
Quanbing Liu,
Guangdong University of Technology, China

Reviewed by:
Yaocai Bai,
Oak Ridge National Laboratory (DOE), United States
Wei Luo,
Wuhan University, China
Hui Wang,
Qingdao University of Science and Technology, China

***Correspondence:**
Xianfeng Li
wind9425@163.com
Liucheng Gui
guiliucheng2000@163.com

Specialty section:
This article was submitted to Catalysis and Photocatalysis, a section of the journal Frontiers in Chemistry

Received: 23 September 2019
Accepted: 28 October 2019
Published: 14 November 2019

Citation:
Li X, Gui L and Zou H (2019) Bracelet-Like $Ni_{0.4}Cu_{0.6}O$ Microstructure Composed of Well-Aligned Nanoplatelets as a Superior Catalyst to the Hydrolysis of Ammonia Borane. Front. Chem. 7:776. doi: 10.3389/fchem.2019.00776

The development of novel catalysts with both high catalytic activity and low cost toward the hydrolysis of ammonia borane is an important subject in the field of hydrogen energy. In this communications, $Ni_xCu_{1-x}O$ microstructures with different morphology have been synthesized and their catalytic activities in AB hydrolysis is studied. It's found that bracelet-like nanoplatelets were obtained at $x = 0.4$ and exhibit highest catalytic performance with turnover frequency of 33.43 $mol_{hydrogen}$ min^{-1} mol_{cat}^{-1}, which much higher than those of most of CuNi-based catalysts in the literature. Pronounced synergistic effects between CuO and NiO in AB hydrolysis also have been observed. Due to the superior catalytic performance and cheapness, the prepared bracelet-like nanoplatelets $Ni_{0.4}Cu_{0.6}O$ catalysts can be a strong catalyst candidate in AB hydrolysis.

Keywords: heterogeneous catalysis, nanoplatelets, hydrogen production, ammonia borane, hydrolysis

INTRODUCTION

Hydrogen is clean energy resource that has attracted extensive attention in the word. It can be regarded as one of the most promising green energy by which we can replace the traditional fossil fuel in view of the high calorific value, zero-emission, as well as renewable characteristics (Liu et al., 2010; Yang et al., 2010). However, how to store and produce hydrogen in safe and efficient way is still big problem in industrial scale applications. So far, many strategies have been developed for dealing with hydrogen storages and production. Among them, hydrolytic dehydrogenation of ammonia borane (AB) by a catalytic process has been deemed as an effective and reliable route (Wang et al., 2016; Du et al., 2017; Men et al., 2018). In this route, the proper catalyst is indispensable due to the slow kinetics of AB hydrolysis in the absence of a catalyst. In the literature, there are two typical types of catalysts toward AB hydrolysis, including noble-metal-based metals and alloys [for examples, Pt (Aijaz et al., 2012), Pd (Xi et al., 2012), Ru (Basu et al., 2009), and their alloy (Amali et al., 2013; Zhou and Xu, 2016)] and cheap metals and alloys [for examples, Co (Yan et al., 2010), Cu (Yao et al., 2014), and their alloys (Li et al., 2015; Bulut et al., 2016; Lu et al., 2018)]. Considering the low cost, the second types of catalysts seem to be more attractive in the practical applications. However, the activity of cheap metals and alloys in AB hydrolysis is far from satisfactory. In this regard, catalysts with both low cost and high catalytic activities are still highly desirable.

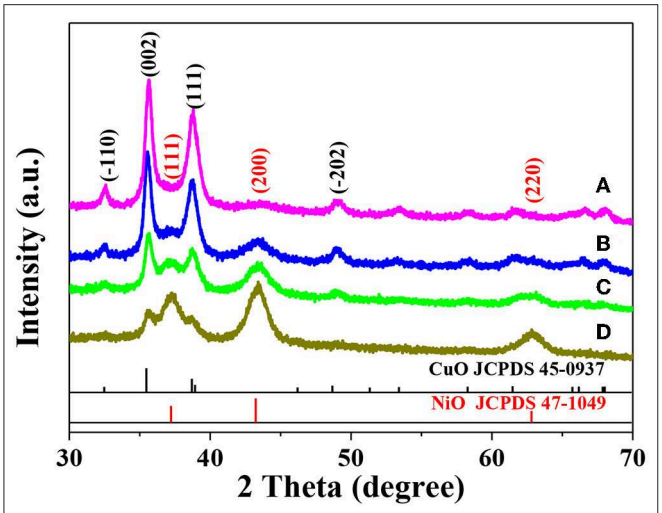

FIGURE 1 | XRD patterns of $Ni_{0.2}Cu_{0.8}O$ **(A)**, $Ni_{0.4}Cu_{0.6}O$ **(B)**, $Ni_{0.6}Cu_{0.4}O$ **(C)**, and $Ni_{0.8}Cu_{0.2}O$ **(D)**.

In this work, a series of nanostructures $Ni_xCu_{1-x}O$ catalysts and their activity in AB hydrolysis have been synthesized and studied. As far as we know, these catalysts used in AB hydrolysis have not been documented in the literature. It's found that the highest catalytic performance can be achieved at x = 0.4. In addition, the pronounced synergistic effects between CuO and NiO in AB hydrolysis have been observed. The findings in the present study can provide insight to help other researchers design inexpensive and highly active catalysts.

RESULTS AND DISCUSSION

Figure 1 shows the XRD patterns of different $Ni_xCu_{1-x}O$ catalysts. As can be seen, the characteristic peaks of both CuO and NiO are observed in these four XRD patterns. Evidently, as x increase, the intensity of peaks related to NiO increase while that of CuO decrease. Notably, it is difficult for us to judge whether the $Ni_xCu_{1-x}O$ is a homogeneous hybrid or just a mixture of CuO and NiO based on the XRD results alone. The XRD patterns of single-component CuO and NiO are shown in **Figures S1a** and **S1b**, respectively. Evidently, the characteristic peaks well match those of standard XRD patterns.

All the $Ni_xCu_{1-x}O$ catalysts are analyzed with SEM and the results are shown in **Figure 2**. **Figure 2a** indicates that $Ni_{0.8}Cu_{0.2}O$ is microspheres composed of nanowires with irradiation arrangement. The diameter of the nanowires is about 30 nm and length is 500–1000 nm. The morphology of $Ni_{0.6}Cu_{0.4}O$ is very similar to that of $Ni_{0.8}Cu_{0.2}O$. Interestingly, the morphology of the products changes remarkably when x = 0.4. As shown in **Figure 2e**, a lot of belt-like agglomeration can be observed, some of which curls like rings. The typical width of the belts is about 2–4 μm. **Figure 2g** clearly indicates that these belts are composed of numerous well-arrayed nanoplatelets with the thickness of around 30 nm. The morphology of the $Ni_{0.2}Cu_{0.8}O$ is similar to that of $Ni_{0.4}Cu_{0.6}O$, but the sizes of the small nanoplatelets become larger. The SEM images of CuO and NiO are displayed in **Figure S2**. CuO is the aggregation of micro-sized nanoplates and NiO is microspheres composed of nanosheets with thickness of about 30 nm. **Figure 3a** shows the TEM images of a part of belt-like agglomeration, confirming that the agglomeration is consisting of plenteous small nanoplatelets. **Figure 3b** indicates that the width of these nanoplatelets is about 500 nm. Notably, we carried out an ultrasonication treatment of the $Ni_{0.4}Cu_{0.6}O$ rings and found that the ultrasonication treatment failed to break the rings into separated nanoplatelets. This finding implied that the $Ni_{0.4}Cu_{0.6}O$ rings are integrative, not consisting of loosely connected nanoplatelets.

Figure 4 displays the SEM image of a belt-like agglomeration and corresponding Cu, Ni, and O mapping. Interestingly, element of Cu, Ni, and O have almost the same mapping, indicating that these elements are uniformly distributed. This observation hints that our $Ni_{0.4}Cu_{0.6}O$ catalyst is a homogeneous hybrid rather than a mixture of CuO and NiO.

The XPS spectra of the $Ni_{0.6}Cu_{0.4}O$ are shown in **Figure 5**. **Figure 5A** is XPS spectrum of the Cu in the 2p region. The peak at 933.2 and 953.3 eV are attributed to the binging energies of Cu 2p 3/2 and Cu 1/2 levels. The splitting of two peaks 20.1 eV, along with their position establishes the presence of CuO (Jana et al., 2010). In **Figure 5B**, the Ni 2p peaks can be decomposed into four peaks at 853.8, 855.6, 871.9, and 872.9 eV, besides the two satellite (Sat.) peaks. The first and third peaks can be ascribed to Ni^{2+} and the second and fourth peak can be assigned to Ni^{3+} (Zhao et al., 2009). Notably, although Ni^{3+} has been detected in the surface of the $Ni_{0.6}Cu_{0.4}O$ sample, no characteristic peaks of Ni_2O_3 has been observed in the XRD pattern. This suggests that there is only a small amount of Ni^{3+} in the surface of the sample. This is understandable because our sample has been calcined during the synthesis, in which the oxidative transformation of Ni^{2+} to Ni^{3+} maybe happen on the surface.

Figure 6A shows the hydrogen evolution from AB solution in the presence of different catalysts. When NiO acts as a catalyst, no hydrogen is released from AB solution, indicating that NiO is inactive to AB hydrolysis. When CuO is used instead, the hydrogen release is quite slow, demonstrating that CuO possesses low catalytic activity. Interestingly, when the $Ni_xCu_{1-x}O$ microstructures serve as catalysts, hydrogen will be produced constantly and fast until the hydrolytic reaction complete. **Figure 6B** shows the TOF for different catalysts. It is found that $Ni_{0.4}Cu_{0.6}O$ exhibit the highest TOF of 33.43 $mol_{hydrogen}\ min^{-1}\ mol_{cat}^{-1}$. In contrast to the CuNi based catalysts in the literature, our $Ni_{0.4}Cu_{0.6}O$ catalyst exhibit significantly improved catalytic activity. This value is higher than that of Cu/RGO (3.61 $mol_{hydrogen}\ min^{-1}\ mol_{cat}^{-1}$) (Yang et al., 2014), nanoporous nickel spheres (19.6 $mol_{hydrogen}\ min^{-1}\ mol_{cat}^{-1}$) (Cao et al., 2010). It is also higher than that of Cu_2Ni_1@MIL-101 (20.9 $mol_{hydrogen}\ min^{-1}\ mol_{cat}^{-1}$) (Gao et al., 2018), CuNi/MCM-41 (15.0 $mol_{hydrogen}\ min^{-1}\ mol_{cat}^{-1}$) (Lu et al., 2014), and CuNi@carbon (0.2 $mol_{hydrogen}\ min^{-1}\ mol_{cat}^{-1}$) (Yousef et al., 2012). However, it is still slightly lower than that of CuNi-CeO_2/graphene oxide recently reported in the literature (34.4 $mol_{hydrogen}\ min^{-1}\ mol_{cat}^{-1}$) (Zhou et al., 2017). Notably, the

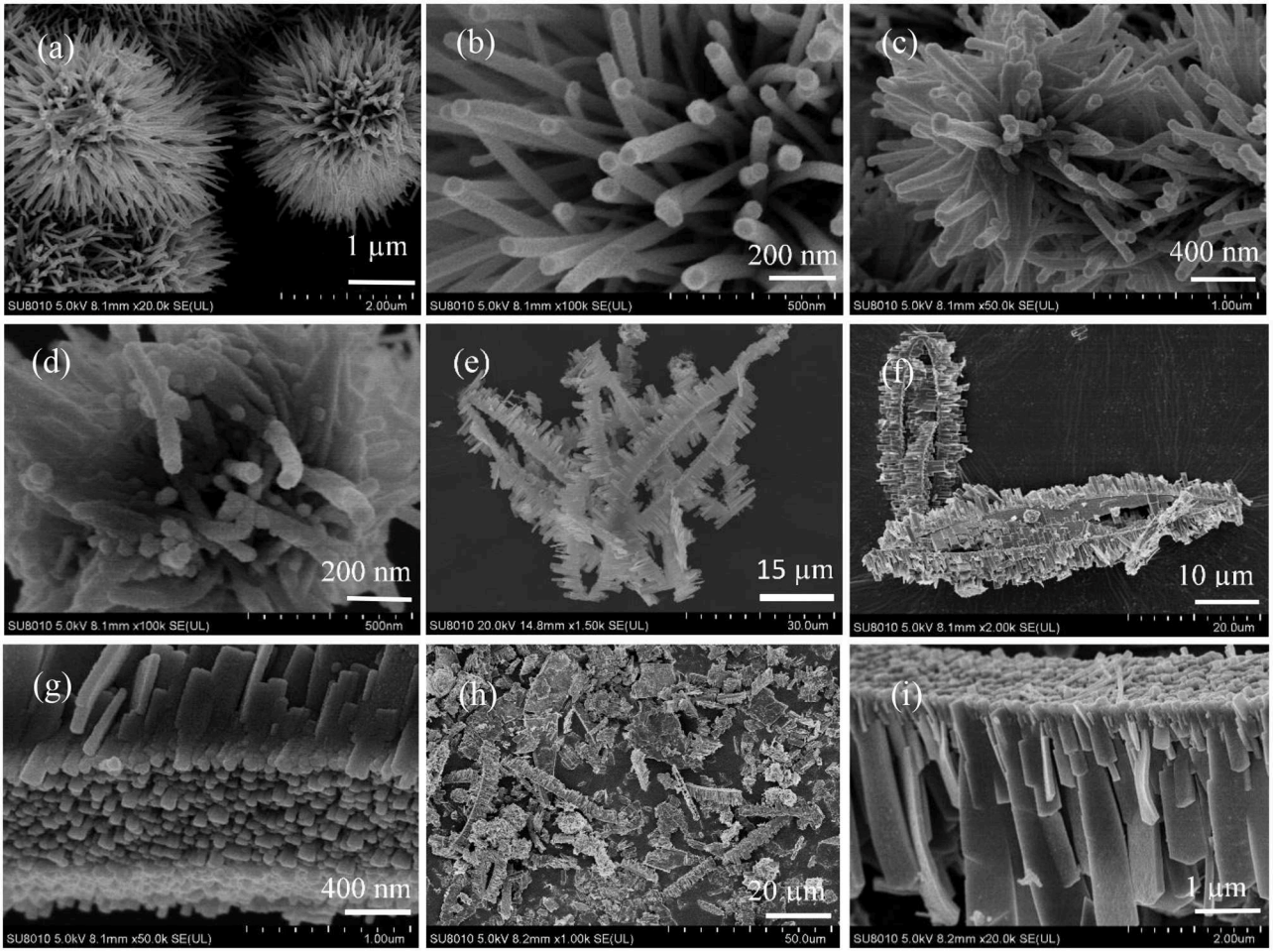

FIGURE 2 | SEM images of $Ni_{0.8}Cu_{0.2}O$ **(a,b)**, $Ni_{0.6}Cu_{0.4}O$ **(c,d)**, $Ni_{0.4}Cu_{0.6}O$ **(e–g)**, and $Ni_{0.2}Cu_{0.8}O$ **(h,i)**.

TOF value for $Ni_xCu_{1-x}O$ is significantly higher than the sum of those for NiO and CuO. This observation hints that there is significant synergistic effect between NiO and CuO in AB hydrolysis. There are two possible reasons for this. Firstly, according to Liao et al. (2018) and Lu et al. (2019), the real active species of oxide-based catalysts is the metals or alloys formed by the reduction of oxides by AB. However, it is difficult to reduce CoO and NiO to their metallic states on account of their low reduction potential (Ni^{2+}/Ni: −0.257 V vs. SHE; Co^{2+}/Co: −0.280 V vs. SHE). When CuO is present, AB can easily reduce CuO to Cu due to the high reduction potential (Cu^{2+}/Cu: 0.337 V vs. SHE), which is favorable for the reduction of CoO and NiO. Thus, active species can be formed immediately. Secondly, the modification of the surface electronic structure and chemical properties of the nanoalloy through the strain and ligand effects between two metals can synergistically improve the catalytic activity (Liao et al., 2018). Notably, our $Ni_{0.6}Cu_{0.4}O$ catalysts is more active than CuNi alloys. As mentioned above, CuNi alloys will be *in-situ* formed on the surface of $Ni_{0.6}Cu_{0.4}O$ catalysts. The unreacted $Ni_{0.6}Cu_{0.4}O$ will act as a support. Thus, there is a metal-support effect within our catalyst. It is possible that the metal-support effect plays an important role in determining their high catalytic activity.

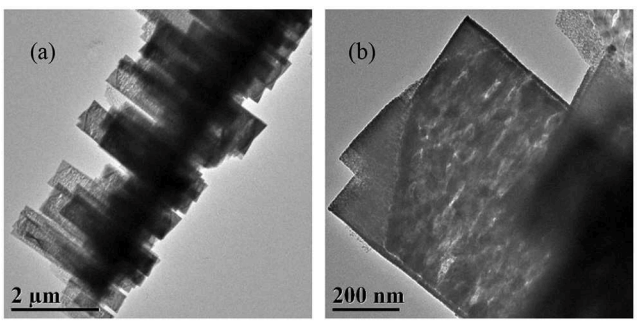

FIGURE 3 | TEM images of $Ni_{0.4}Cu_{0.6}O$ catalyst with low **(a)** and high **(b)** magnification.

To investigate the amount of catalyst on the hydrogen generation rate, catalytic hydrolysis of AB catalyzed by

different catalyst dosage is carried out. As can be seen in **Figure 7A**, the hydrogen generation rate becomes larger and larger when the catalyst dosage increases in the range from 5.0 to 12.5 mg. This is understandable because more active sites are provided for the adsorption of AB in the presence of larger catalyst dosage. To further clarify the relationship between the hydrogen generation rate (r) and the catalyst dosage (m), ln$r$ vs. ln$m$ was plotted in **Figure 7B**. The slope of the fitted line is 0.89, very close to 1, indicating that AB hydrolysis is a pseudo first-order reaction with respect to the catalyst. Thus, the hydrogen generation rate can be easily controlled by adjusting the catalyst dosage in the practical applications.

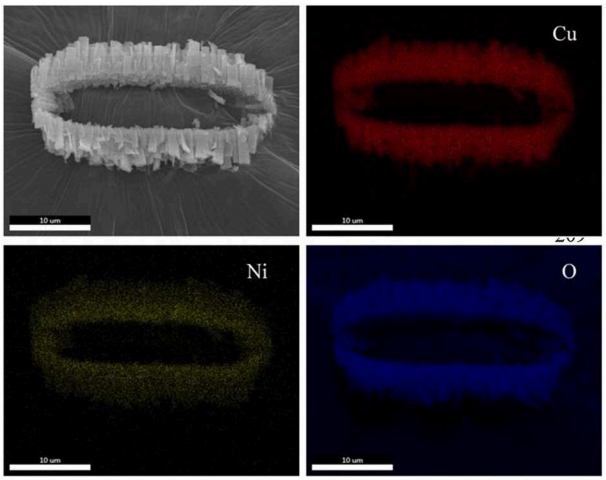

FIGURE 4 | Elemental mapping of $Ni_{0.4}Cu_{0.6}O$ catalyst.

Besides the hydrogen generation rate, apparent activation energy is another important parameter that can be applied to roughly assess the catalytic activity of a catalyst. In general, an active catalyst can significantly lower the reaction energy barrier (apparent activation energy) and thus increase the reaction rate. Correspondingly, low apparent activation energy of a catalytic reaction reflects that the catalyst possesses high catalytic activity. In **Figure 8A**, hydrogen evolution curves at different reaction temperature are displayed. Obviously, higher reaction temperature leads to faster hydrogen generation rate. By plotting lnk vs. ln(1/T), a fitted straight

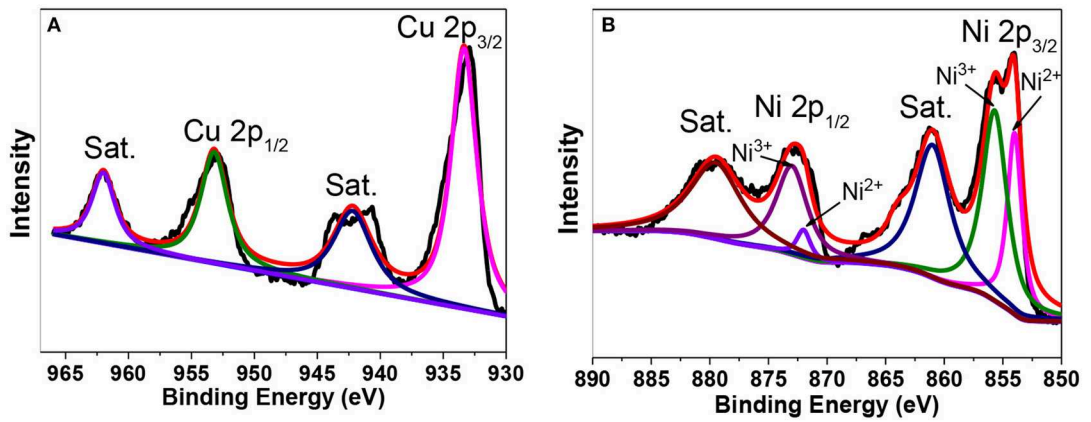

FIGURE 5 | XPS spectra of Cu 2p **(A)** and Ni 2p **(B)**.

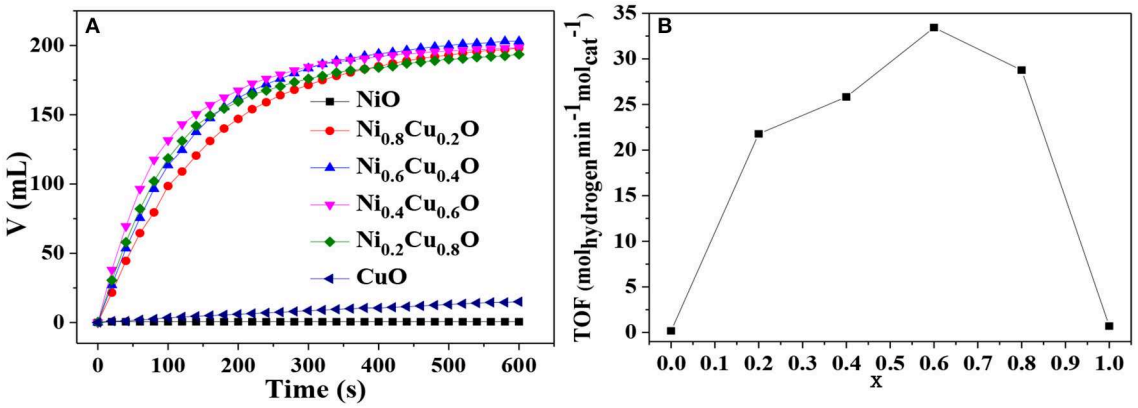

FIGURE 6 | (A) Hydrogen release from AB solution in the presence of different catalyst and **(B)** TOF values vs. x in $Ni_xCu_{1-x}O$.

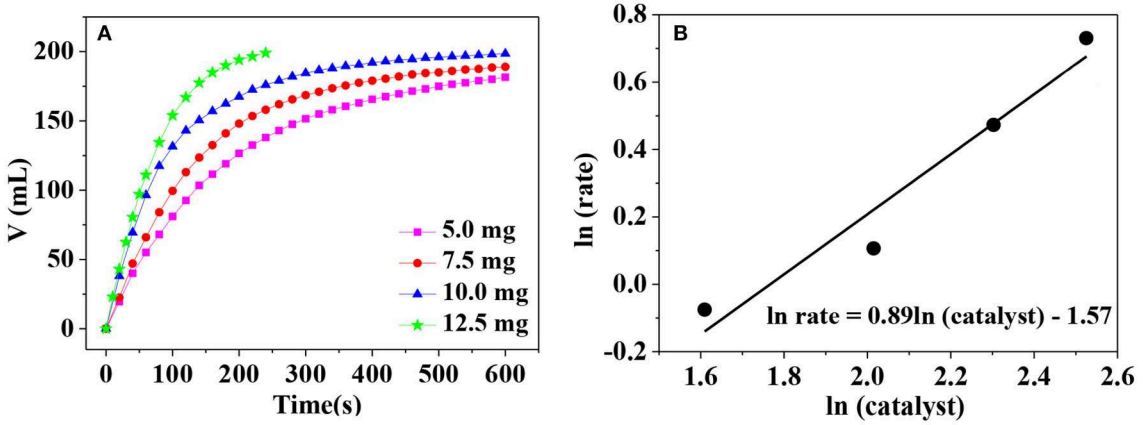

FIGURE 7 | (A) Hydrogen release from AB solution at different catalyst dosage; **(B)** the relationship between logarithm of mass of catalyst and catalytic rate.

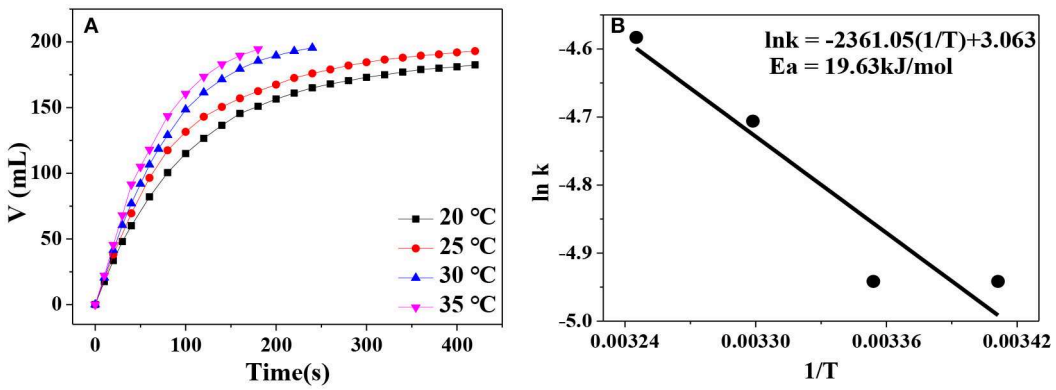

FIGURE 8 | (A) Hydrogen evolution at various catalytic temperature in the range of 20–35°C; **(B)** the relationship between logarithm of k and 1/T.

line is generated. According to the Arrhenius equation, the apparent activation energy of AB hydrolysis for our $Ni_{0.4}Cu_{0.6}O$ catalyst is calculated to be about 19.63 kJ/mol (**Figure 8B**), which is lower than that of CuNi/MCM-41 (38 kJ/mol) (Lu et al., 2014) and Cu_2Ni_1@MIL-101 (32.2 kJ/mol) (Gao et al., 2018).

To investigate the stability and reusability of the $Ni_{0.4}Cu_{0.6}O$ catalyst, the catalytic hydrolysis reaction was carried out repeatedly. As shown in **Figure 9**, the molar ratio of hydrogen to AB is 3 at the fifth catalytic run, verifying that the 100% hydrogen release ratio can be achieved. However, the catalyst activity of the catalyst decreases slightly after 5 catalytic runs. The SEM image of the used catalyst in **Figure S3** indicates that the morphology of used catalyst remains almost unchanged. These findings demonstrate $Ni_{0.4}Cu_{0.6}O$ catalyst have good reusability and relatively high stability.

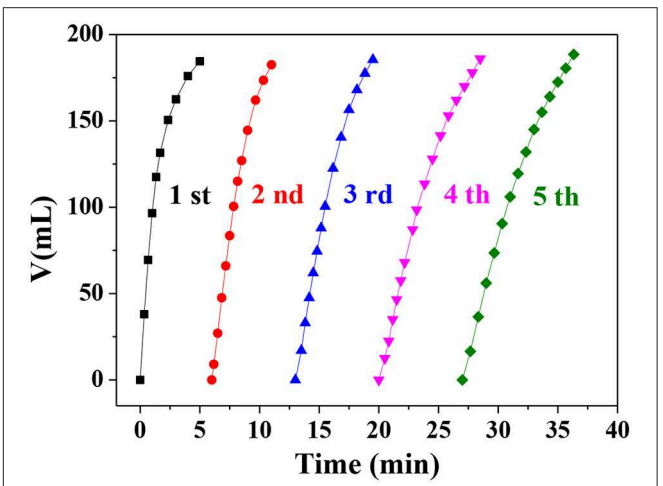

FIGURE 9 | The hydrogen evolution at various catalytic cycles.

CONCLUSION

In summary, nanostructured $Ni_xCu_{1-x}O$ cat with different morphology have been prepared and their catalytic activity in AB hydrolysis has been studied. It is found that the belt-like $Ni_{0.4}Cu_{0.6}O$ composed of plenteous well-aligned nanoplatelet exhibit the highest catalytic performance with turnover frequency of 33.43 $mol_{hydrogen}$ min^{-1} mol_{cat}^{-1}, which

is much higher than that of most of CuNi-based catalysts in the literature. It is interesting to note that there is pronounced synergistic effect between CuO and NiO in AB hydrolysis. Owing to its superior catalytic performance and cheapness, the $Ni_{0.4}Cu_{0.6}O$ catalysts can be strong catalyst candidate in AB hydrolysis.

Synthesis

All of the reagents are of analytic grade. In a typical process, $CuSO_4 \cdot 5H_2O$ and $NiSO_4 \cdot 6H_2O$ with a total metal ions of 5.0 mmol were dissolved in 20 mL water to form solution A. Twenty millimole urea was dissolved in 20 mL water to form solution B and 1.0 g cetyltrimethylammonium bromide (CTAB) was dissolved in 40 mL water to form solution C. After solution A and B were mixed, solution C was added to the mixture solution under stirring. After that, the resulted solution was poured in to a Teflon-lined autoclave, which was sealed and subjected to a heat-treatment at 160°C for 10 h. The solid product obtained at the bottom of the Teflon-lined autoclave was washed and calcined at 400°C for 4 h.

Characterizations

Rigaku D/Max-1200X diffractometer with Cu Kα radiation was applied to record the X-ray powder diffraction (XRD) patterns of the samples. Hitachi Su-8010 field emission scanning electron microscope (FE-SEM) was used to analyze the morphology of the samples. Elemental mapping analysis was carried out using an EDAX Octane Elite energy disperse spectrometer (EDS) coupled with FE-SEM. Transmission electron microscopy (TEM) and high-resolution TEM (HRTEM) images were obtained on a FEI Tecnai G2 F20 S-TWIN transmission electron microscope. X-ray photoelectron spectroscopy (XPS) was performed on a Kratos Axis Ultra DLD X-ray photoelectron spectrometer with Al Kα radiation.

Catalytic Experiments

In a typical experiment, catalyst with weight of 10.0 mg was dispersed into 10.0 mL water under ultrasonication. Then, 10 mL mixed solution of AB (0.3 M) and NaOH (2 M) was added into the vessel, which was sealed and connected to a glass burette. NaOH was used in the catalytic process because it could enhance AB hydrolysis (Yan et al., 2016). The reaction vessel was immersed into a water bath at temperature of 298 K. The volume of the produced hydrogen was determined by recording the displacement of water in the gas burette.

DATA AVAILABILITY STATEMENT

The datasets generated for this study are available on request to the corresponding author.

AUTHOR CONTRIBUTIONS

Synthesis of the sample, writing-original draft preparation, and investigation of the catalytic performance were performed by XL. Characterization and analysis of the sample by XL and LG. Supervision, funding acquisition and writing-review, and editing by XL and HZ. All authors have given their approval to the final version of the manuscript.

FUNDING

This work was supported by Huizhou University Leading Academic Discipline Project.

SUPPLEMENTARY MATERIAL

The Supplementary Material for this article can be found online at: https://www.frontiersin.org/articles/10.3389/fchem.2019.00776/full#supplementary-material

REFERENCES

Aijaz, A., Karkamkar, A., Choi, Y. J., Tsumori, N., Ronnebro, E., Autrey, T., et al. (2012). Immobilizing highly catalytically active Pt nanoparticles inside the pores of metal-organic framework: a double solvents approach. *J. Am. Chem. Soc.* 134, 13926–13929. doi: 10.1021/ja3043905

Amali, A. J., Aranishi, K., Uchida, T., and Xu, Q. (2013). PdPt nanocubes: a high-performance catalyst for hydrolytic dehydrogenation of ammonia borane. *Part. Part. Syst. Charact.* 30, 888–892. doi: 10.1002/ppsc.201300100

Basu, S., Brockman, A., Gagare, P., Zheng, Y., Ramachandran, P. V., Delgass, W. N., et al. (2009). Chemical kinetics of Ru-catalyzed ammonia borane hydrolysis. *J. Pow. Sour.* 188, 238–243. doi: 10.1016/j.jpowsour.2008.11.085

Bulut, A., Yurderi, M., Ertas, I. E., Celebi, M., Kaya, M., and Zahmakiran, M. (2016). Carbon dispersed copper-cobalt alloy nanoparticles: a cost-effective heterogeneous catalyst with exceptional performance in the hydrolytic dehydrogenation of ammonia-borane. *Appl. Catal. B Environ.* 180, 121–129. doi: 10.1016/j.apcatb.2015.06.021

Cao, C.-Y., Chen, C.-Q., Li, W., Song, W.-G., and Cai, W. (2010). Nanoporous nickel spheres as highly active catalyst for hydrogen generation from ammonia borane. *ChemSusChem* 3, 1241–1244. doi: 10.1002/cssc.201000229

Du, X., Yang, C., Zeng, X., Wu, T., Zhou, Y., Cai, P., Cheng, G., et al. (2017). Amorphous NiP supported on rGO for superior hydrogen generation from hydrolysis of ammonia borane. *Int. J. Hydrogen Energy* 42, 14181–14187. doi: 10.1016/j.ijhydene.2017.04.052

Gao, D., Zhang, Y., Zhou, L., and Yang, K. (2018). CuNi NPs supported on MIL-101 as highly active catalysts for the hydrolysis of ammonia borane. *Appl. Surface Sci.* 427, 114–122. doi: 10.1016/j.apsusc.2017.08.167

Jana, S., Das, S., Das, N. S., and Chattopadhyay, K. K. (2010). CuO nanostructures on copper foil by a simple wet chemical route at room temperature. *Mater. Res. Bull.* 45, 693–698. doi: 10.1016/j.materresbull.2010.02.014

Li, J., Zhu, Q. L., and Xu, Q. (2015). Non-noble bimetallic CuCo nanoparticles encapsulated in the pores of metal–organic frameworks: synergetic catalysis in the hydrolysis of ammonia borane for hydrogen generation. *Catal. Sci. Technol.* 5, 525–530. doi: 10.1039/C4CY01049C

Liao, J. Y., Lu,. D. S., Diao, G. Q., Zhang, X. B., Zhao, M. N., and Li, H. (2018). $Co_{0.8}Cu_{0.2}MoO_4$ microspheres composed of nanoplatelets as a robust catalyst for the hydrolysis of ammonia borane. *ACS Sustainable Chem. Eng.* 6, 5843–5851. doi: 10.1021/acssuschemeng.7b03994

Liu, C., Li, F., Ma, L. P., and Cheng, H. M. (2010). Advanced materials for energy storage. *Adv. Mater.* 22, E28–E62. doi: 10.1002/adma.200903328

Lu, D. S., Li, J. H., Lin, C. H., Liao, J. Y., Feng, Y. F., Ding, Z. T., et al. (2019). A simple and scalable route to synthesize $Co_xCu_{1-x}Co_2O_4$@$Co_yCu_{1-y}Co_2O_4$ yolk–shell microspheres, a high-performance catalyst to hydrolyze

ammonia borane for hydrogen production. *Small* 15:1805460. doi: 10.1002/smll.201805460

Lu, D. S., Liao, J. Y., Zhong, S. D., Leng, Y., Ji, S., Wang, H., et al. (2018). $Cu_{0.6}Ni_{0.4}Co_2O_4$ nanowires, a novel noble-metal free catalyst with ultrahigh catalytic activity towards the hydrolysis of ammonia borane for hydrogen production. *Int. J. Hydrogen Energy* 43, 5541–5550. doi: 10.1016/j.ijhydene.2018.01.129

Lu, Z. H., Li, J., Feng, G., Yao, Q., Zhang, F., Zhou, R., et al. (2014). Synergistic catalysis of MCM-41 immobilized Cu–Ni nanoparticles in hydrolytic dehydrogeneration of ammonia borane. *Int. J. Hydrogen Energy* 39, 13389–13395. doi: 10.1016/j.ijhydene.2014.04.086

Men, Y., Su, J., Huang, C., Liang, L., Cai, P., Cheng, G., et al. (2018). Three-dimensional nitrogen-doped graphene hydrogel supported Co-CeO_x nanoclusters as efficient catalysts for hydrogen generation from hydrolysis of ammonia borane. *Chin. Chem. Lett.* 29, 1671–1674. doi: 10.1016/j.cclet.2018.04.009

Wang, X., Liao, J., Li, H., Wang, H., and Wang, R. (2016). Solid-state-reaction synthesis of cotton-like CoB alloy at room temperature as a catalyst for hydrogen generation. *J. Colloid Interface Sci.* 475, 149–153. doi: 10.1016/j.jcis.2016.04.033

Xi, P., Chen, F., Xie, G., Ma, C., Liu, H., Shao, C., et al. (2012). Surfactant free RGO/Pd nanocomposites as highly active heterogeneous catalysts for the hydrolytic dehydrogenation of ammonia borane for chemical hydrogen storage. *Nanoscale* 4, 5597–5601. doi: 10.1039/c2nr31010d

Yan, J., Liao, J. Y., Li, H., Wang, H., and Wang, R. F. (2016). Magnetic field induced synthesis of amorphous CoB alloy nanowires as a highly active catalyst for hydrogen generation from ammonia borane. *Catal. Commun.* 84, 124–128. doi: 10.1016/j.catcom.2016.06.019

Yan, J. M., Zhang, X. B., Shioyama, H., and Xu, Q. (2010). Room temperature hydrolytic dehydrogenation of ammonia borane catalyzed by Co nanoparticles. *J. Pow. Sour.* 195, 1091–1094. doi: 10.1016/j.jpowsour.2009.08.067

Yang, J., Sudik, A., Wolverton, C., and Siegel, D. J. (2010). High capacity hydrogen storage materials: attributes for automotive applications and techniques for materials discovery. *Chem. Soc. Rev.* 39, 656–675. doi: 10.1039/B802882F

Yang, Y. W., Lu, Z. H., Hu, Y. J., Zhang, Z. J., Shi, W. M., Chen, X. S., et al. (2014). Facile in situ synthesis of copper nanoparticles supported on graphene for hydrolytic dehydrogenation of ammonia borane. *RSC Adv.* 4, 13749–13752. doi: 10.1039/C3RA47023G

Yao, Q., Lu, Z. H., Zhang, Z., Chen, X., and Lan, Y. (2014). One-pot synthesis of core-shell Cu@SiO_2 nanospheres and their catalysis for hydrolytic dehydrogenation of ammonia borane and hydrazine borane. *Sci. Rep.* 4:7597. doi: 10.1038/srep07597

Yousef, A., Barakat, N. A. M., El-Newehy, M., and Kim, H. Y. (2012). Chemically stable electrospun NiCu nanorods@carbon naofibers for highly efficient dehydrogenation of ammonia borane. *Int. J. Hydrogen Energy* 37, 17715–17723. doi: 10.1016/j.ijhydene.2012.09.038

Zhao, B., Ke, X. K., Bao, J. H., Wang, C. L., Dong, L., Chen, Y. W., et al. (2009). Synthesis of flower-like NiO and effects of morphology on its catalytic properties. *J. Phys. Chem. C* 113, 14440–14447. doi: 10.1021/jp904186k

Zhou, Q., and Xu, C. (2016). Nanoporous PtRu alloys with unique catalytic activity toward hydrolytic dehydrogenation of ammonia borane. *Chem. Asian J.* 11, 705–712. doi: 10.1002/asia.201500970

Zhou, Y. H., Wang, S., Wan, Y., Liang, J., Chen, Y., Luo, S., et al. (2017). Low-cost CuNi-CeO_2/rGO as an efficient catalyst for hydrolysis of ammonia borane and tandem reduction of 4-nitrophenol. *J. Alloys Comp.* 728, 902–909. doi: 10.1016/j.jallcom.2017.09.075

Conflict of Interest: The authors declare that the research was conducted in the absence of any commercial or financial relationships that could be construed as a potential conflict of interest.